Available online at www.sciencedirect.com
SCIENCE DIRECT®
Journal of Power Sources 122 (2003) 28–36
JOURNAL OF POWER SOURCES
www.elsevier.com/locate/jpowsour

Study of multistage oxidation by flowsheet calculations on a combined heat and power molten carbonate fuel cell plant

S.F. Au [a,b,*], N. Woudstra [b], K. Hemmes [c]

[a] Delft University of Technology, Laboratory of Material Science, Rotterdamseweg 137, 2628 AL Delft, The Netherlands
[b] Delft University of Technology, Laboratory for Thermal Power Engineering, Mekelweg 2, 2628 CD Delft, The Netherlands
[c] Delft University of Technology, Faculty of Technology, Policy and Management, P.O. Box 5015, 2600 GA Delft, The Netherlands

Received 22 August 2002; received in revised form 3 February 2003; accepted 10 February 2003

Abstract

The multistage oxidation configuration consists of a set of serially connected fuel cell stacks. By connecting the stacks serially, more homogenous current distribution over the cell surface can be achieved resulting in lower irreversible losses.

This article presents a detailed assessment of multistage oxidation by flowsheet calculations in which the influence of operating temperature and gas composition on the fuel cell performance is incorporated. A 250 kW molten carbonate fuel cell (MCFC) combined heat and power (CHP) plant is used as reference and the fuel cell stack unit is substituted by two serially connected units ($N = 2$). Two multistage configurations are examined: (A) both anode and cathode flows are serially connected; (B) only the anode flow is serially connected while the cathode flow is parallel connected. For all systems, the total cell active area, cell current density, overall fuel utilization and gas temperature at the inlet and outlet of the fuel cell array are kept constant. Fuel cell performance at the operating conditions is calculated using a numerical model of the flowsheeting program. Influences of operating temperature and gas composition on the cell performance are incorporated using empirical relations that describe irreversible losses of the cell as function of these parameters. System performances are compared in order to assess the benefits of the multistage oxidation configurations. Differences in performance between the two multistage oxidation configurations are studied by analyzing the difference in exergy loss of stacks, stack power output, cooling requirement and cathode gas massflow and composition.

Detailed flowsheet calculations show that the improvement in efficiency is about 0.6% for configuration A, and 0.8% for configuration B. Improvements are obtained by the enhanced fuel cell power output while the expander power output is slightly reduced. Heat output is slightly reduced due to the improved fuel cell conversion. Analysis of stack output revealed a intricate interaction between stack and the rest of the fuel cell system. Their mutual influences are examined and the results explain differences in results between configuration A and B.

Keywords: Flowsheet; Fuel cell system; Exergy

1. Introduction

Previously [1], we have introduced a one-dimensional fuel cell model based on the equivalent circuit given in Fig. 1. Here, we assume that inside the cell the difference between the local Nernst voltage $V_{eq}(x)$ and the uniform cell voltage V_{cell} is the driving force to overcome all irreversible losses (i.e. ionic/electronic conductance and activation/diffusion polarization) lumped into the uniform quasi-ohmic resistance r. Conversion of gaseous reactant inside the cell causes a gas composition gradient between the fuel cell gas inlet and outlet and a similar gradient in the $V_{eq}(x)$ exists between the gas inlet and outlet. The quasi-ohmic resistance r is by definition uniform over the cell, therefore this gradient in $V_{eq}(x)$ results in an inhomogeneous conversion and current density inside the cell (see Fig. 2). Conversion of the gaseous reactant is high at the fuel cell gas inlet where $V_{rev}(x)$ is high, while the conversion rate is lower at the gas outlet where $V_{rev}(x)$ is low. This inhomogeneous conversion rate is equivalent to an inhomogeneous current distribution and this adversely affects the fuel cells performance [2].

The multistage oxidation configuration consists of a set of serially connected fuel cell stacks. By connecting the stacks in series, more homogenous current distribution over the cell surface can be achieved resulting in lower polarization losses [2] (see Fig. 2). Standaert and coworkers [2,3]

* Corresponding author. Present address: Institute for Materials and Process in Energy Systems, IWV3 Energy Process Engineering, Forschungszentrum Jülich, Jülich D-52425, Germany.
Tel.: +49-2461-615291; fax: +49-2461-616695.
E-mail address: s.f.au@fz-juelich.de (S.F. Au).

0378-7753/03/$ – see front matter
doi:10.1016/S0378-7753(03)00346-X

Nomenclature

A_{cell}	active cell area (m^2)
C	fitting constant for quasi-ohmic resistance ($\Omega\,m^2$)
d	electrolyte thickness (mm)
d_b	normalization constant for the electrolyte thickness (mm)
Ex_{loss}	exergy loss (kW)
Δh	change in enthalpy (J/mol)
i_{cell}	fuel cell current density (A/m^2)
m_i	molar fraction of specie i
p	pressure (bar)
Δp	pressure loss (bar)
p_i	partial pressure of specie i (bar)
$\tilde{P}_{cell}$	power density (kW/m^2)
ΔT_{low}	low end temperature difference of heat exchanger (K)
T_{cell}	fuel cell temperature (°C)
r	quasi-ohmic resistance ($\Omega\,m^2$)
R	universal gas constant (J/(mol K))
u_f	total fuel utilization
V_{cell}	cell voltage (V)
V_{eq}	theoretical Nernst potential (V)

Greek letters

Φ	massflow (kg/s)
η_{dc-ac}	dc to ac inverter efficiency
η_i	intrinsic efficiency
η_{Ex}	exergy efficiency based exergy of fuel input and $T_0 = 25\,°C$
η_{th}	thermal efficiency based on lower heating value of fuel input

have previously analytically examined the thermodynamic principle of multistage oxidation and he found an analytical expression for the gain in power density w (W/cm^2) as function of number of segments N [3]:

$$w(N) = \frac{1}{12}\frac{(\alpha u_f)^2}{r}\left(1 - \frac{1}{N^2}\right) \quad (1)$$

with r ($\Omega\,cm^2$) the quasi-ohmic resistance, α (V) the slope of the linearized Nernst equation and u_f the fuel utilization.

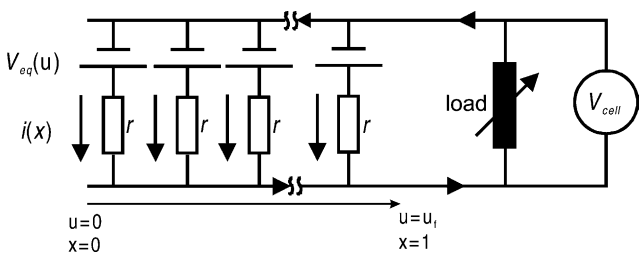

Fig. 1. Fuel cell represented as an equivalent electrical circuit.

For the molten carbonate fuel cell (MCFC), it is shown that an improvement in electric efficiency of about 1% can be achieved by splitting the cell area into $N = 2$ segments [3]. This conclusion was based on both analytical mathematical modeling and simplified flowsheet calculations. Liebhafsky and Cairns [4] and Selimovic and Palsson [5] both have also considered the use of multistage oxidation, but then for the solid oxide fuel cell (SOFC). They showed that an improvement in power output of about 5% point can be obtained for their systems. In the above mentioned studies, the influence of temperature and gas composition on the polarization losses was previously neglected. Recent studies show that the cell resistance depends strongly on the operating temperature of the stack [6,7]. Furthermore, our recent study [8] has shown that the complex interactions between fuel cell stack and auxiliary equipments additionally complicate system evaluations. More realistic and detailed flowsheet calculations are therefore required to further assess the benefit of multistage oxidation in system performance in practice. Selimovic and Plasson [5] recently presented a flowsheet study in which they investigated the implementation of multistage oxidation on a SOFC gas turbine (GT) hybrid system. They found an 18% increase in fuel cell power output and 5% increase in total system efficiency. These results are obtained by changing the cell configuration from one-stage to multi-stage oxidation and simultaneously increasing the total fuel utilization u_f of the fuel cells. Since u_f is an important parameter for the fuel cell performance, the final result cannot be solely ascribed to the change in cell configuration and additional studies are required.

2. System calculations

The MCFC-combined heat and power (CHP) reference system selected for this study has the following main features:

- 250 kW class MCFC stack;
- heat production at two temperature levels (saturated steam at 180 °C and hot water at 80 °C);
- natural gas as primary fuel (equivalent to 557.57 kW LHV);
- fuel gas is externally reformed;
- pressurized system operating at 4 bar.

Fig. 3 shows the flowsheet of the system. Apart from the fuel cell stack (apparatus #11), this system can be distinguished in five subsystems, as shown in the figure. This MCFC-CHP system is used for another article [8] in which the influence of operating temperature on the system is studied. This article contains a detailed description of this system to which further information are referred [8]. For the input parameters for apparatus, we used inputs data that characterize state-of-the-art equipments. The overall performance of this MCFC-CHP plant and the multistage oxidation

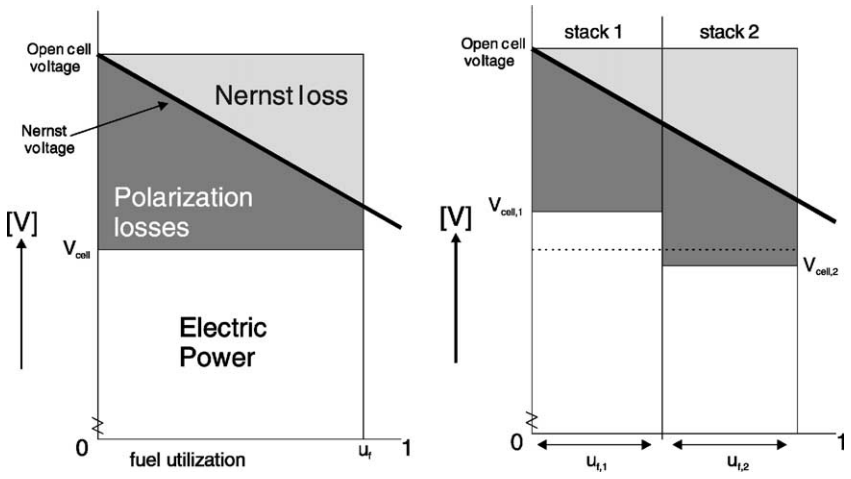

Fig. 2. Schematic representation of the polarization losses of the stack before and after splitting it into two segments, taken from [2].

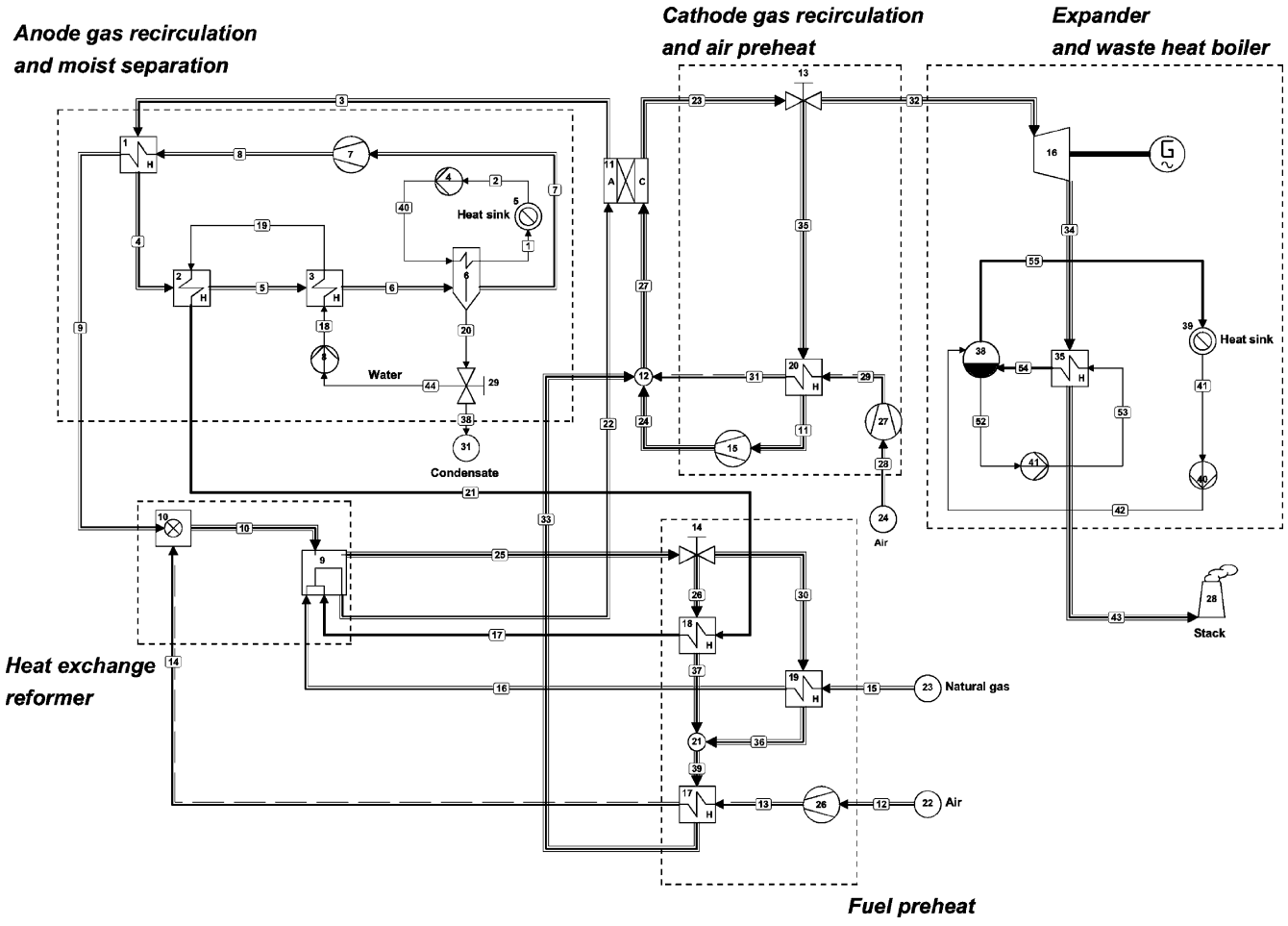

Fig. 3. Flowsheet of the 250 kW-class MCFC CHP plant.

derivatives are calculated by the flowsheet program Cycle-Tempo [9].

The standard average operating temperature of 650 °C is used here as a reference. Table 1 gives the operating parameters of the MCFC stacks. These inputs represent the operating condition and characteristics of state of the art MCFC stacks at full load. The cell resistance r of the fuel cell stack is calculated using the empirical relations [6,7] determined by CRIEPI.[1] They have determined the cell resistance as

[1] Central Research Institute of Electric Power Industry, Japan.

Table 1
Input parameters of the fuel cell stack of the reference stack and sub-stacks of multistage oxidation systems

	Reference	Multistage A		Multistage B	
	MCFC stack	First sub-stack A1	Second sub-stack A2	First sub-stack B1	Second sub-stack B2
T_{cell} (°C)	650	Calculated	Calculated	650	650
p (bar)	4	4	4	4	4
u_f (%)	70	35	53.85	35	53.85
A_{cell} (m^2)	250	125	125	125	125
i_{cell} (A/m^2)	1500	1500	1500	1500	1500
r ($\Omega\,cm^2$)	0.6072	Calculated	Calculated	Calculated	Calculated
$T_{out}-T_{in}$ (°C)	100	Calculated	Calculated	100	100
Δp_{anode} (bar)	0.05	0.025	0.025	0.025	0.025
$\Delta p_{cathode}$ (bar)	0.1	0.05	0.05	0.1	0.1
η_{dc-ac} (%)	96	96	96	96	96

functions of the average cell temperature T_{cell}, operating pressure p, and the average gas composition at both the anode and cathode (by means of average partial pressures p_i and mol fractions m_i). The empirical relations and the fitting values are summarized in [8].

The calculated cell resistance is used in the numerical fuel cell model of the flowsheeting program to calculate the fuel cell performance (characterized by the cell voltage V_{cell}). This model is the numerical implementation of the equivalent circuit of the fuel cell process given in Fig. 1. Next to this cell performance calculation (containing both calculations of reversible heat production and ohmic- and reaction kinetics-losses), the numerical model also calculates the mass and energy transfers between the anode and cathode massflows, gas heating and power output. Hence, this numerical model simulates the complete fuel cell operation at any operating condition using the cell resistance r as the cell performance characterization parameter. A detailed description and assessment of the accuracy of this numerical model is given in [10].

The fuel cell stack of the reference system, given in Fig. 3, is here split into two equal segments, while anode flows are connected in series (see Fig. 4). These two serially connected sub-stacks represent multistage oxidation with $N = 2$. Each sub-stack has an active cell area that is half of the reference stack. The active cell area, pressure losses and current density are the same for both sub-stacks. The cumulative fuel utilization u_f of the complete stack unit is shared equally by the two sub-stacks. The fuel utilization u_f is defined with respect to the fuel input at the cell inlet. Since the second stack is fed with leaner fuel than the first stack, u_f of each sub-stack is therefore different by definition. The fuel utilization of the reference stack is 70%. Therefore, the fuel utilization of the first sub-stack of the multistage system is 35% while according to the definition the second sub-stack is operating at a fuel utilization of 53.85%[2] relative to the inlet of the second sub-stack. With these stack operating-parameters, the anode massflow and the overall fuel utilization of two sub-stacks together are kept the same as for the stack of the reference system. Note that the fuel utilization of this reference system is relatively low and that the gain in power density by multistage oxidation is proportioned to the fuel utilization (see Eq. (1)). It is however not possible to increase the fuel utilization without significantly modifying the reference system hence the fuel utilization is kept at 70%.

Two configuration of multistage oxidation are examined (see Fig. 4):

- Multistage A: cathode flows of the two sub-stacks are connected *serially*.
- Multistage B: cathode flows of the two sub-stacks are connected in *parallel*.

Multistage A resembles the original fuel cell stack simply devised into two sub-stacks. Multistage B on the other hand is also devised but may need some additional changes in the cathode pipe arrangement. It is important to note that the sub-stacks in both configurations are electrically disconnected allowing both stacks to have different stack voltages and power densities accordingly to their operating conditions. Having the anode massflow connected serially, both configurations represent multistage oxidation and only the cathode flows are different.

Other difference between Multistages A and B is the operating temperature of the stack. This difference is the result of a combination of boundary conditions and the cooling principle of the stacks. In order to solely assess the effect of multistage oxidation, it is crucial to keep the rest of the system the same as much as possible and the inlet and outlet temperature of the stack unit should therefore be kept the same in all case. The inlet temperature of the first sub-stack in both Multistages A and B is therefore set at 600 °C and the outlet temperature of the second sub-stack is set at 700 °C. This boundary condition results in a difference between the two multistage configurations in the mean average temperature of the sub-stacks. All stacks are cooled by the cathode massflow resulting in a temperature difference between the inlet and outlet. Since the cathode flow of Multistage A is serially

[2] The ratio of 0.35/(1−0.35).

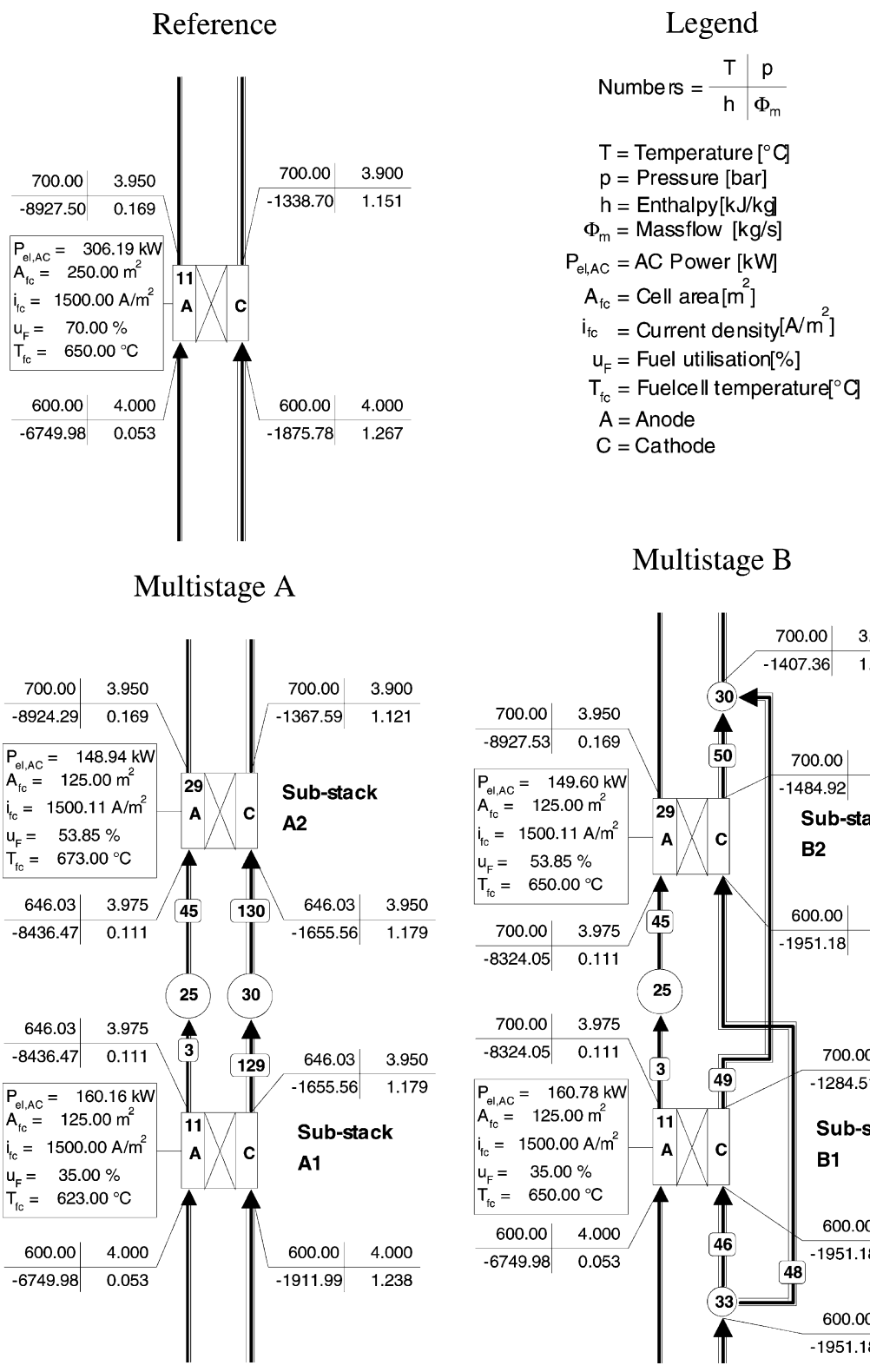

Fig. 4. The reference single stack unit and the two multistage configurations.

connected, the intermediate temperature between the two sub-stack is somewhere between 600 and 700 °C and the operating temperature[3] of each sub-stacks is therefore different. Multistage B does not have the cathode flow serially connected but instead they are both joint together forming the stack unit's outlet. The outlet temperatures of the cathode of the sub-stacks are taken the same as the reference stack. For the anode flow, it is assumed that it is heated up only at the first sub-stack while it is kept constant in the second sub-stack. Since the anode flow is relatively low compared to the cathode flow, it is assumed that the stack operating temperature is solely determined by the average cathode temperature. Hence, both sub-stacks operate at the same temperature as the reference stack. Fig. 4 shows the differences in stack configuration and cathode outlet temperatures.

The flowsheet calculation of the Multistage B system is analogous to that of the reference system, and the calculation is described in details in our previous paper [8]. The calculation of the flowsheet for Multistage A is somewhat different since the operating temperature of the sub-stacks are calculated instead of defined by the designer. For this, we need to calculate the intermediate temperature between the first and the second sub-stack. This intermediate temperature is calculated by the flowsheeting program by solving the energy and mass balances of the stacks using the numerical solving routine of the program. The numerical solving routine allows two options for the user to fulfill the energy and mass balances. The first option is that the temperature increase of the flows through the cell is specified, resulting in the calculation of the cathode massflow.[4] The second option allows specifying the cathode massflow; then the temperature increase ($T_{out} - T_{in}$) is calculated. The combination of both options solves the energy and mass balances of the stack unit and determines the operating temperatures of the sub-stacks. The first option is used for the second sub-stack; this determines the cathode massflow of both sub-stacks. The second option is used for the first sub-stack; this determines the stack's outlet temperature, which is the inlet temperature of the second stack. The combination of both options enables the program to iteratively determine the intermediate temperature between the two stacks. As in the reference system, the operating temperatures of the (sub) stacks are assumed to be the mean average of the in and outlet.

The operating temperatures of the stacks are determined using the calculations by the program. However, the fuel cell model of the program requires the input of both cell temperature and cell resistance for calculating the performance of the sub-stacks. Both inputs should be given prior to each flowsheet iteration. It is obvious that the stack performance determines the cooling requirement of the stack, and for system A it also determines the operating temperature via the intermediate temperature between the two sub-stacks. In other words, intermediate temperature, stack operating temperatures, cell resistances[5] and stack performance are all coupled and the stack operating temperatures and cell resistances can only be determined by iterative steps until conversion is reached. Since these iterative steps were not programmed in the flowsheeting program, numerous manual iterations are required before the solution is found that satisfies both the flowsheet results and the separately calculated cell resistances.

The input parameters of the reference and multistage oxidation fuel cell stacks are summarized in Table 1.

Table 2
Energy output and efficiencies of the reference and multistage systems

	Reference	Multistage A	Multistage B
FC stack output (kW)	306.19	A1: 160.16 A2: 148.94 Total: 309.10	B1: 160.78 B2: 149.60 Total: 310.38
Expander (kW)	60.05	58.71	58.09
Auxiliary (kW)	−77.58	−75.97	−75.20
Net power (kW)	288.66	291.84	293.27
η_{th} (%)	51.77	52.34 (+0.57)	52.60 (+0.83)
η_{Ex} (%)	49.70	50.25 (+0.55)	50.49 (+0.79)
$Heat_{T=180\,°C}$ (kW)	91.59	89.66	88.84
$Heat_{T=80\,°C}$ (kW)	109.49	110.22	109.49
Total output (kW)	489.74	491.72	491.59
η_{th} (%)	87.84	88.19 (+0.35)	88.17 (+0.33)
η_{Ex} (%)	58.46	58.90 (+0.44)	59.08 (+0.62)

3. Results and discussion

3.1. Net power efficiencies

Table 2 gives the energy and exergy outputs and efficiencies of the systems. For the multistage configurations, the improvements in efficiencies over the reference system are given between brackets. Here, we should note that the numbers in the tables are given in two digits behind the decimal point. This suggests a high level of precision in our computer simulations. On the other hand, we have used several approximated input values for the performance of heat exchangers and rotating equipment and consequently the absolute value in the calculated efficiencies have no practical values. Nevertheless, these numbers are not round off since here we are only interested in the difference in the calculated results, which will not become apparent otherwise.

Table 2 shows that both multistage oxidation systems perform better than the reference system and that system B is

[3] The mean average temperature between the stack inlet and outlet is assumed as the operating temperature of the stack.

[4] Both fuel utilization and anode mass flow should be given. This is compulsory in Cycle-Tempo, thus the cathode massflow is determined by the cooling of the stack.

[5] The cell resistances are calculated using a spreadsheet program with the CRIEPI empirical relations given in [8].

the best performing system of the three. By splitting up the fuel cell stack, the stack output increases with 2.9 kW for system A, and 4.2 kW for system B (see the differences in Table 2). Simultaneously, the auxiliary power consumption decreases with 1.7 kW for system A and 1.9 kW for system B. However, the expander power output decreases with 1.3 kW for system A, and 2.0 kW for system B. Hence, we see here a levelling effect in the overall system efficiencies: an increase in stack power output results to a decrease in heat release by the stack thus a lower power output by the heat recovery expander. Overall, the improvement in both thermal efficiency η_{th} and exergy efficiency η_{Ex} are here in the order of 0.6% point for system A and 0.8% point for system B. The improvements in system efficiencies are clearly less than the improvements in stack outputs.

A similar leveling effect has also occurred in the fuel cell stacks and we have analyzed this by examining the data of the stacks.

3.2. Improvements by multistage oxidation

Starting with Multistage A, the intermediate temperature for the two sub-stacks of Multistage A is calculated as 648 °C (see Fig. 4). With this, the average operating temperatures for the sub-stacks are 623 and 673 °C for respectively first and second sub-stacks. The irreversible losses of the cell depend strongly on the operating temperature and this is represented by the difference in cell resistance r (see Table 3). The first sub-stack A1 is operating at a relatively low temperature resulting in a high r. Vice versa, the second sub-stack A2 is operating at a relatively high temperature resulting in a low r. Comparing to the reference stack, the cell resistance r of A1 is about 33% higher than the reference stack. This means an increase in irreversible losses, which adversely affects the stack performance. Nevertheless, the net power output density $\tilde{P}_{cell}$ of this sub-stack is about 5% higher than the reference stack (1.281 kW/m^2 versus 1.225 kW/m^2, see Table 3). This paradox is a direct result of the multistage oxidation concept and it is caused by the lower Nernst loss of this stack (see Fig. 2, and [2] for more details). A similar paradox holds for the second stack. The cell resistance of A2 stack is about 14% lower than the reference stack but the power density of this stack is about 3% lower compared to the reference stack. Here, the difference is caused by the leaner fuel. The net power output of both stacks combined is 2.91 kW (or 0.52% point η_{th}) higher than the reference stack. More chemical energy is therefore converted into electric power and less heat is produced. The enhanced conversion efficiency reduces the cooling requirement of the stack hence lowering the cathode massflow $\Phi_{cathode}$ (see Table 3). Combined with the lower input of air that can be seen from the lower expander massflow $\Phi_{expander}$ given in Table 3, the result is a decrease in auxiliary power consumption of 1.61 kW (see Table 2). On the other hand, the reduced expander massflow results in a reduction of power output by the generator of 1.34 kW. The overall result is an increase of 3.18 kW to the total net power production, which amounts to a relative increase of 1.1% with respect to the reference system. Based on the input of fuel, this results in an increase of net efficiency of 0.57% point and 0.55% based on respectively η_{th} and η_{Ex}. Hence, Multistage A performs slightly better than the reference system.

Table 3
Stack data, and cathode recycling data and gas composition

	Reference	Multistage A	Multistage B
T_{cell} (°C)	650	A1: 623 A2: 673	B1: 650 B2: 650
r (Ω cm^2)	0.6072	A1: 0.8082 A2: 0.5246	A1: 0.6224 A2: 0.6212
Ex_{loss} (kW)	25.86	A1: 14.15 A2: 10.80 Total:24.95	A1: 12.29 A2: 12.05 Total: 24.34
$\tilde{P}_{cell}$ (kW/m^2)	1.225	A1: 1.281 A2: 1.192	A1: 1.286 A2: 1.197
$\Phi_{cathode}$ (kg/s)	1.267	1.238	A1: 0.489 A2: 0.740 Total: 1.229
$\Phi_{expander}$ (kg/s)	0.264	0.258	0.255
$\%_{recycling}$	77.09	77.01	77.10
$\bar{p}_{O_2}$ (bar)	0.228	A1: 0.237 A2: 0.198	B1: 0.197 B2: 0.216
$\bar{p}_{CO_2}$ (bar)	0.385	A1: 0.435 A2: 0.355	B1: 0.375 B2: 0.412
$\bar{m}_{H_2O}$	0.119	A1: 0.117 A2: 0.122	B1: 0.124 B2: 0.122

The increase in net performance by Multistage B is even more than Multistage A. Here, the increase in power output of both sub-stacks combined is 4.19 kW (or 0.75% point η_{th}) versus reference, and 1.28 kW (or 0.23% point η_{th}) versus Multistage A (see Table 2). We have analyzed the differences using the stack data given in Table 3, and in particular the difference between Multistages A and B. For Multistage B, we have used the typical 650 °C for the operating temperature of both sub-stacks. Since the operating temperature of both stacks is the same as the reference, the cell resistances of both stacks are of the same order (see Table 3). This results in a more even distribution of exergy losses over the two stacks compared to. Multistage A. Hence, the total exergy loss for Multistage B is lower than Multistage A (see Table 3). The cell resistances for both sub-stacks of Multistage B are still slightly higher than the reference stack. The differences are caused by the differences in the cathode gas composition.[6] The cathode gas compositions are given in Table 3 and they are calculated by the program. The situation here is very complex since the cathode gas composition is influenced both by the cooling requirement of the

[6] The contribution of the anode to the total cell resistance is relatively small.

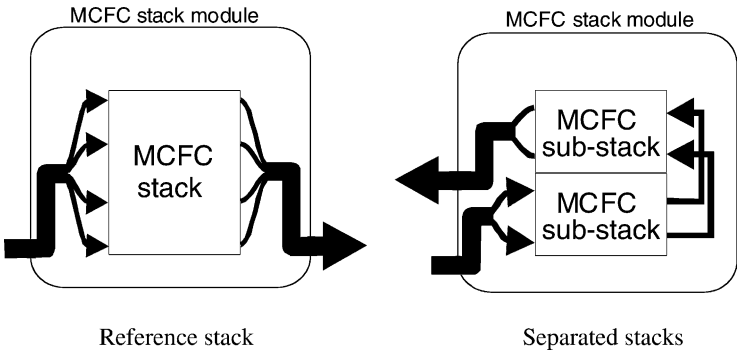

Fig. 5. Separating stack to multistage oxidation with $N = 2$.

stack (given by Φ_{cathode}), and by the heat requirement of the fresh air (given here $\%_{\text{recycling}}$). The complex interactions and their results cannot be predicted by theory. What we observed here is an increase in fuel cell stack irreversibility (higher r) due to increase in stack power output. Hence, this system shows a leveling effect in the increase of stack power output. It is an excellent example of the unpredictable characteristics of fuel cell systems.

3.3. Overall CHP efficiencies

Table 2 also summarizes the heat output of the systems. The multistage systems produce less heat in the form of super heated steam at $T = 180\,^{\circ}\text{C}$ than the reference system. This follows directly from the improved efficiency of the fuel cell stacks. Since the increase in stack output is more for Multistage B than Multistage A, thus less super heated steam is produced by B than by A. Heat output in the form of steam is about the same. For Multistage A, the slightly increased output of hot water at $T = 80\,^{\circ}\text{C}$ is caused by the differences in gas composition at the outlet of the anode. This difference results from the higher operating temperature of the second sub-stack with respect to the other systems (675 °C for A2 while the others operate at 650 °C). This increase in operating temperature alters the chemical equilibrium of the hydrogen shift reaction and therefore the outlet gas composition. The resulting difference in water vapor content of the anode offgas explains the small difference in low temperature heat output of both systems.

Overall, the net CHP performances of the multistage oxidation systems are higher than the reference system. For Multistage A, the increases in efficiencies are 0.35 and 0.44% point for respectively η_{th} and η_{Ex}. For Multistage B, the increases in efficiencies are 0.33 and 0.62% point for respectively η_{th} and η_{Ex}.

3.4. Comparison with previous works and discussions

The present multistage oxidation system is different from the system used previously by Standaert [3] and a direct comparison of results is hence not possible. For example Standaert's reference system has a net electrical efficiency of 47% point versus 52% point here (both based on η_{th}). Nevertheless, when comparing the improvement of multi-stage oxidation, our present results are lower than the results of Standaert [3]. Standaert's calculations suggest an improvement of about 1% in net efficiency for Multistage A configuration, while our present detailed calculations show that about 0.6% improvement in net power output is more realistic. The relatively low fuel utilization of this system may have contributed in the lower system improvement.

Our present results are also less optimistic compared to the result from Selimovic and Palsson [5]. Furthermore, this study shows an additional gain in overall net efficiency by parallel cathode flow, as done here with Multistage B. The latter contradicts the results presented by Selimovic and Palsson [5]. However, we should note that the previous results were obtained by changing simultaneously both system layout and fuel cell operating parameters. Especially the changes in fuel utilization u_{f} and current density i_{cell} have significant impact on the fuel cell stack performance. Therefore, again our present results cannot be directly compared with the results from their previous study [5].

Finally, we will make some remarks regarding the application of multistage oxidation in practice. Splitting up the fuel cell stack seems to involve significant changes in the design and manufacturing of fuel cell stacks. In practice, it is more likely that the multistage oxidation as presented here only involves a rearrangement of piping. State of the art MCFC-stack modules that are currently used in pilot plants consist of two small size sub-stacks that are fed parallel. An example is the IHI[7] 250 kW MCFC stack unit [12], built for the 1 MW pilot plant [13] in Kawagoe, Japan. Multistage oxidation configuration can be obtained by simply connecting the sub-stacks in series instead of parallel (see Fig. 5). Since the power plants itself often consists of several stack units as well, these units can also be placed in series providing another alternative for multistage oxidation. In the Multistage A configuration, the temperature difference between the gas inlets and outlets of each sub-stack is also reduced, which may improve endurance and reduction of production cost.

[7] Ishikawajima-Harima Heavy Industries Co. Ltd.

Lastly, multistage oxidation configuration allows additionally the implementation of intermediate cooling and fuel injection between the two sub-stacks as proposed in [11]. These features require significant changes in system layout making the assessment on the effect of multistage oxidation less transparent. These system changes are hence here omitted and the possible improvements by these two changes should be addressed in the future.

4. Conclusion

A gain in performance is achieved by implementing multistage oxidation instead of parallel connection of stacks. Detailed flowsheet calculations show that the improvement in net efficiency is about 0.6% when both anode and cathode flows are place in series. Additional 0.3% point improvement can be obtained by placing solely the anode flow in series while keeping the cathode flow parallel. Both configurations enhance fuel cell power output while reducing slightly the expander power output. The total heat output is also slightly reduced. Overall, the net power thermal efficiency (based on LHV) of this 250 kW class CHP MCFC plant is increased from 51.8 to 52.3% by placing both anode and cathode flows in series, and to 52.6% by placing solely the anode flow in series. Based on exergy, the net efficiency increases from 49.7 to 50.3% for both flows in series, and 50.5% for solely the anode in series. The increase in total CHP efficiency is slightly lower. Based on exergy, the CHP efficiency increases from 58.5 to 58.9% for both flows in series, and 59.1% for solely the anode in series. These improvements can simply be obtained by rearranging piping in state of the art modular fuel cell systems, which are currently being tested in pilot plants.

This study has again shown the intricate interaction between the fuel cell stack and the rest of the system. Improvement in fuel cell conversion not only increases the fuel cell stack output but it also reduced auxiliary power consumption by reduced cooling requirement. Less cooling translates to lower cathode massflow, which increases oxidant utilization and hinders reaction kinetics. The latter results to increase in irreversible losses and thus adversely affects cell performance. Hence, it is not possible to translate improvement in stack performance directly to improvements in overall system performance. The results in these complex situations can only be revealed by detailed flowsheet calculations as presented by this study.

References

[1] S.F. Au, W.H.A. Peelen, F.R.A.M. Standaert, K. Hemmes, I. Uchida, Verification of Analytical Fuel Cell Models by Performance Testing at a 110 cm^2 Molten Carbonate Fuel Cell, Pennington, NJ, USA, 2000, pp. A1051–A1057, J. Electrochem. Soc.148 (10).
[2] F. Standaert, K. Hemmes, N. Woudstra, Nernst loss and multistage oxidation in fuel cells, in: Proceedings of the Fuel Cell Seminar, 16–19 November 1998, Palm Spring, California, USA, pp. 92–95.
[3] F. Standeart, Analytical Fuel Cell Modelling and Exergy Analysis of Fuel Cells, Ph.D. Thesis, Delft University of Technology, 1998.
[4] H.A. Liebhafsky, E.J. Cairns, Fuel Cells and Fuel Batteries, Wiley, New York, 1968.
[5] A. Selimovic, J. Palsson, Networked solid oxide fuel cell stacks combined with a gas turbine cycle, J. Power Sources 106 (2002) 76–82.
[6] F. Yoshiba, N. Ono, Y. Izaki, T. Watanabe, T. Abe, Numerical analyses of the internal condition of a molten carbonate fuel cell stack: comparison of stack performances for various gas flow types, J. Power Sources 71 (1998) 328–336.
[7] Y. Mugikura, H. Morita, M. Yoshikawa, T. Watanabe, Modification of cathode performance equation and reaction mechanism of MCFC, in: Proceeding of the 7th FCDIC Fuel Cell Symposium, Tokyo, Japan, 2000.
[8] S.F. Au, S.J. McPhail, N. Woudstra, K. Hemmes, The influence of operating temperature on the efficiency of a combined heat and power fuel cell plant, J. Power Sources 122 (2003) 37–46.
[9] Cycle-Tempo version 4.42, Delft University of Technology, Section Thermal Power Engineering TNO Environment, Energy and Process Innovation, 2000, http://www-pe.wbmt.tudelft.nl/ev/cycle/cycle.html.
[10] S.F. Au, N. Woudstra, K. Hemmes, I. Uchida, Verification of a simple numerical model in a flowsheeting program by performance testing at a 110 cm^2 molten carbonate fuel cell, Energy Conv. Manage., in press.
[11] J.G. Wimer, M.C. Williams, Molten Carbonate Fuel Cell Networks: Principles, Analysis, and Performance, Springfield, NTIS, 1993.
[12] T. Ogawa, A. Matsunaga, T. Matsuyama, H. Kasai, K. Miyazawa, Evaluation of 250 kW MCFC stack for 1000 kW MCFC Power plant, Abstracts of the Fuel Cell Seminar, 2000.
[13] Y. Izaki, H. Yasue, Demonstration of the first 1000 kW MCFC power plant in Japan, Abstracts of the Fuel Cell Seminar, 2000.